JVI Accepted Manuscript Posted Online 6 January 2016
J. Virol. doi:10.1128/JVI.03036-15

Activation of RNase L by murine coronavirus in myeloid cells is dependent on basal *Oas* gene expression and independent of virus-induced interferon

L. Dillon Birdwell[1], Zachary B. Zalinger[1], Yize Li[1], Patrick W. Wright[2], Ruth Elliott[1], Kristine M. Rose[1,*], Robert H. Silverman[3], and Susan R. Weiss[1,#]

[1]Department of Microbiology, Perelman School of Medicine, University of Pennsylvania, Philadelphia, PA, [2]Department of Biomedical Engineering, Washington University in St. Louis, St. Louis, MO and [3]Department of Cancer Biology, Cleveland Clinic, Cleveland, OH

Running title: RNase L activation depends on basal *Oas* expression

[*]present address:
PATH
455 Massachusetts Avenue NW, Suite 1000
Washington, DC 20001

[#]Address correspondence to:

Susan R. Weiss
Department of Microbiology
University of Pennsylvania
School of Medicine
203A Johnson Pavilion
36th Street and Hamilton Walk
Philadelphia, PA 19104-6076
Phone: 215-898-8013
Email: weisssr@upenn.edu

Abstract number of words: 238

Text number of words: 6320

ABSTRACT

The oligoadenylate synthetase-ribonuclease L (OAS-RNase L) pathway is a potent interferon (IFN) induced antiviral activity. Upon sensing double stranded RNA, OAS produces 2',5'-oligoadenylates (2-5A), which activate RNase L. Murine coronavirus (MHV) non-structural protein 2 (ns2), is a 2',5'-phosphodiesterase (PDE) that cleaves 2-5A, thereby antagonizing RNase L activation. PDE activity is required for robust replication in myeloid cells as a mutant of MHV (ns2^{H126R}) encoding an inactive PDE fails to antagonize RNase L activation and replicates poorly in bone marrow derived macrophages (BMM) while ns2^{H126R} replicates to high titer in several types of non-myeloid cells as well as in IFN receptor deficient (*Ifnar1*$^{-/-}$) BMM. We reported previously that myeloid cells express significantly higher basal levels of Oas transcripts than non-myeloid cells. Here, we investigated the contributions of *Oas* gene expression, basal IFN signaling and virus-induced IFN to RNase L activation. Infection with ns2^{H126R} activated RNase L in *Ifih1*$^{-/-}$ BMM to a similar extent as in WT BMM despite the lack of IFN induction in the absence of MDA5 expression. However, ns2^{H126R} failed to induce RNase L activation in BMM treated with IFNAR1 blocking antibody as well as in *Ifnar1*$^{-/-}$ BMM, both expressing low basal levels of *Oas* genes. Thus, activation of RNase L does not require virus-induced IFN, but rather correlates with adequate levels of basal *Oas* gene expression, maintained by basal IFN signaling. Finally, overexpression of RNase L is not sufficient to compensate for inadequate basal OAS levels.

53 **IMPORTANCE**

54 The oligoadenylate-ribonuclease L (OAS-RNase L) pathway is a potent antiviral activity. Activation
55 of RNase L during murine coronavirus, MHV, infection of myeloid cells correlates with high basal
56 *Oas* gene expression and is independent of virus-induced interferon secretion. Thus, our data
57 suggest that cells with high basal *Oas* gene expression levels can activate RNase L and thereby
58 inhibit virus replication early in infection upon exposure to viral dsRNA, before the induction of
59 interferon and prior to transcription of interferon stimulated antiviral genes. These findings challenge
60 the notion that activation of the OAS/RNase L pathway requires virus to induce type I IFN which in
61 turn upregulates OAS gene expression as well as to provide dsRNA to activate OAS. Our data
62 further suggest that myeloid cells may serve as sentinels to restrict viral replication thus protecting
63 other cell types from infection.

64

65 **INTRODUCTION**

66 The coronavirus mouse hepatitis virus (MHV) strain A59 (A59) causes moderate hepatitis
67 and mild encephalitis followed by chronic demyelinating disease in susceptible C57BL/6 (B6) mice
68 (1-3). A59 is cleared from the liver and central nervous system primarily by the T cell response
69 seven to ten days post infection (4,5). However, type I interferon (IFN) production, an early innate
70 immune response, is crucial for early control of MHV infection as mice deficient in type I IFN
71 receptor expression (*Ifnar1*$^{-/-}$) uniformly die by two days after infection (6-8). Interestingly, A59 fails
72 to induce IFNα/β in most cell types, with the notable exception of myeloid cells (7). Induction of
73 IFNα/β in macrophages and brain-resident microglia during MHV infection is dependent on sensing
74 of viral dsRNA by the cytosolic RNA helicase, melanoma differentiation-associated gene 5 (MDA5)
75 encoded by *Ifih1* (7,9,10). IFN induces a large array of interferon-stimulated genes (ISGs), which
76 include pattern recognition receptors (PRRs), signaling molecules, transcription factors, and antiviral
77 effectors (11-16). (Figure 1, left side diagrams IFN synthesis and signaling in MHV infected
78 macrophages). The only other source of type I IFN during A59 infection, primarily IFNα, is induced
79 through a TLR7-dependent pathway in plasmacytoid dendritic cells (pDC) (17).

80 Among the ISGs are several *Oas* genes encoding proteins that function as nucleic acid
81 sensors to synthesize 2',5'-oligoadenylates (2-5A) in response to viral dsRNA in the host cytosol
82 (18). Mice express several OAS proteins that produce 2-5A, including OAS1a/g, OAS2, OAS3 as
83 well as OASL2 (19-21). The 2-5A binds to and activates latent ribonuclease L (RNase L) by inducing
84 conformational changes and subsequent dimerization (11,13,22). RNase L activation leads to
85 restriction of virus replication through the degradation of host and viral single stranded RNAs,
86 inhibition of protein synthesis and finally apoptosis (14,23,24). (Figure 1, right side diagrams
87 activation of RNase L).

88 Interactions of viruses with the OAS-RNase L pathway are complex. Many viruses encode
89 proteins that inhibit this pathway to various extents, underscoring the significance of this system in

restricting viral propagation (13,25-28). Among the most potent of these inhibitors is the A59 accessory protein, non-structural protein 2 (ns2), a 2',5'-phosphodiesterase (PDE) that cleaves 2-5A thereby preventing RNase L activation (25). An A59 mutant (ns2^{H126R}) expressing an inactive PDE (due to an H126R substitution of a catalytic histidine residue) fails to effectively antagonize RNase L, and consequently is attenuated for replication in myeloid cells and in the livers of mice (25).

We have found that RNase L activation is most robust in myeloid lineage cells, where basal *Oas* gene expression levels are highest compared with several other types of non-myeloid primary cells including astrocytes, neurons, and oligodendrocytes, as well as transformed cell lines (29). Constitutive, low level type I IFN production in the absence of infection maintains basal levels of expression of ISGs, including OAS (30,31). It has been generally accepted that RNase L activation requires viral infection to both induce type I IFN production which in turns upregulates OAS gene expression and to provide dsRNA for activation of OAS to produce 2-5A (13). Thus, unlike most other IFN-induced activities, which can be stimulated in uninfected cells by paracrine IFN exposure, RNase L can be activated only in infected cells.

To further elucidate the cell-type dependent determinants of RNase L activation, we investigated basal *Oas* mRNA expression, basal IFN signaling, and viral induction of IFN as three potential contributors. Our data indicate that RNase L activation depends on relatively high basal mRNA expression levels of *Oas* genes typical of myeloid cells and overexpression of RNase L is not sufficient to overcome insufficient levels of OAS. Furthermore, RNase L activation requires adequate basal IFN signaling to maintain basal *Oas* mRNA expression. However, in contrast to the current paradigm, RNase L activation does not require IFN induction during virus infection of macrophages. These data suggests that myeloid cells can activate RNase L early during infection and before the induction of IFN and thereby limit viral spread to other cell types.

MATERIALS AND METHODS

116 **Viruses, cell lines, and mice**. Murine L2 fibroblasts were maintained in Dulbecco's modified
117 Eagle's medium (DMEM) supplemented with 10% fetal bovine serum (FBS), HEPES (10 mM), and
118 1% penicillin-streptomycin. Plaque assays were performed on L2 cells as described previously (32).
119 Murine 3T3/pLZ fibroblasts and control 3T3/neo (33) were grown in DMEM containing 10% FBS
120 supplemented with G418 (350 µg/mL) and 1% penicillin-streptomycin. The recombinant
121 coronaviruses inf-MHV-A59 (wild type A59, referred to as A59 here) and inf-ns2-H126R (referred to
122 as $ns2^{H126R}$ here) were obtained from Dr. Stuart Siddell (University of Bristol, Bristol, United
123 Kingdom) and have been described previously (2,34). Newcastle disease virus expressing green
124 fluorescent protein (NDV-GFP) (7,29,35) was obtained from Dr. Luis Martinez-Sobrido (University of
125 Rochester School of Medicine). C57BL/6 (B6) mice were purchased from the National Cancer
126 Institute (Frederick, MD). *Rnasel*$^{-/-}$ mice (bred for 10 generations to obtain a B6 background) were
127 described previously (14). *Ifih1*$^{-/-}$ (36) and *Ifnar1*$^{-/-}$ (37) mice, both with B6 background, were obtained
128 from Dr. Michael S. Diamond (Washington University in St. Louis, St. Louis, MO). Both strains were
129 further bred and maintained in the animal facility at the University of Pennsylvania.
130
131 **qRT-PCR**. RNA was isolated with an RNeasy minikit (Qiagen, Valencia, CA). Quantitative real-time
132 reverse transcriptase-PCR (qRT-PCR) was performed as described previously (2). Briefly, 200 ng
133 (cells) or 350 ng (tissue) of total RNA was reverse transcribed into cDNA using reverse transcriptase
134 (Superscript III; Invitrogen) in a total volume of 20 µL. Then, 2 µL of cDNA was combined with 12.5
135 µL of iQ5 SYBR green mix (Bio-Rad, Hercules, CA), 6.5 µL diethyl pyrocarbonate (DEPC)-treated
136 water, and 4 µL primer mix (5 µM each). DNA was amplified using an iQ5 iCycler (Bio-Rad), and
137 cycle threshold (CT) values were recorded. Expression levels of mRNA were quantified as ΔC_T
138 values relative to β-actin mRNA with the equation: $2^{-\Delta C_T}$, where $\Delta C_T = (C_{T,\ \text{Target Gene}} - C_{T,\ \beta\text{-actin}})$.
139 Quantitative RT-PCR primer sequences are available upon request.
140
141 **Primary cell cultures.** (i) Bone marrow-derived macrophages (BMM) were generated from the hind

142 limbs of B6 (WT), *Ifih1*$^{-/-}$, or *Ifnar1*$^{-/-}$ mice as described previously (25,38,39) and cultured in DMEM
143 supplemented with 10% FBS and 30% L929 cell-conditioned medium for 6 days before infection.
144 Cultures were routinely ≥99% pure as assessed by positive staining for expression of CD11b and
145 negative staining for expression of CD11c. (ii) Bone marrow-derived dendritic cells (BMDC) were
146 generated from the hind limbs of WT mice as described by (40,41) and cultured in RPMI 1640
147 (Sigma-Aldrich) supplemented with 10% FBS, 2 mM L-glutamine, 1% penicillin-streptomycin, 50 μM
148 β-mercaptoethanol, and 20 ng/mL of GM-CSF (Peprotech). The cells were fed on day 3, 6, and 8
149 with fresh media and supplements. On day 10, cells were harvested and replated at 200,000
150 cells/well using growth media with 5 ng/mL GM-CSF on 24-well non-tissue culture treated plates and
151 used for infections. Cells were routinely >95% CD11c^{+} and 80 to 90% immature (MHCII^{lo}). (iii)
152 Hippocampal neurons were prepared from embryonic day 15.5 (E15 to E16) mouse embryos as
153 described previously (42). Briefly, cells were seeded onto poly-L-lysine-coated tissue culture plates,
154 cultured in neurobasal medium containing B-27 supplement (Invitrogen), 1% penicillin-streptomycin,
155 2 mM L-glutamine, and 4 μg/mL glutamate for 4 days in the absence of an astrocyte feeder layer
156 and then used for infections. Neuron cultures were routinely 95 to 98% pure, as determined by
157 positive immunostaining for MAP2 and negative immunostaining for CD11b (microglia-specific
158 marker), glial fibrillary acidic protein (GFAP) (astrocyte-specific marker), and OLIG2
159 (oligodendrocyte-specific marker) (42). (iv) Mixed glial cultures, consisting of astrocytes and
160 microglia, were generated from the brains of 1 to 3-day-old neonatal mice as describe previously
161 (25). Briefly, tissue was dissociated by mechanical disruption through a 70 μm nylon mesh filter and
162 plated in complete medium consisting of DMEM supplemented with 10% FBS, 1% nonessential
163 amino acid solution, 2 mM L-glutamine, 1% penicillin-streptomycin, and 10 mM HEPES and cultured
164 for 9 to 11 days. These cells were lifted from their culture vessel using the enzyme-free, Hank's-
165 based balanced salt solution cell disassociation buffer (Gibco). (v) Astrocyte cultures were
166 generated as described in (iv) and after 9 to 11 days in culture, the flasks were shaken to remove
167 nonadherent microglial cells, and the remaining adherent cells were ≥95% pure astrocytes, as

168 determined by positive immunostaining for GFAP (25) and used for infection. The protocols were
169 approved by the Institutional Animal Care and Use Committee at the University of Pennsylvania.
170
171 **Infections of cell cultures**. Virus was added to cells at a multiplicity of infection (MOI) of 1 PFU/cell
172 and allowed to adsorb for 1 hour at 37 °C. Cultures were washed with PBS (3 times) and fed with
173 medium as described for each cell type. The culture supernatants were harvested at the times
174 indicated for the specific experiments, and the titers were determined by plaque assay on L2 cells.
175
176 **Treatment with IFN and 2-5A**. Cells were treated with 100 units/mL universal IFNα for four hours.
177 Cells were transfected with HPLC purified 10 μM 2-5A (p3A3) in 3 ug/mL Lipofectamine 2000
178 (Invitrogen) or Lipofectamine alone and four hours later cell lysates harvested and RNA isolated.
179
180 **IFNAR1 blocking antibody treatment.** BMM cultures were treated with 0, 2, or 5 μg/mL of
181 IFNAR1blocking mAb (clone MAR1-5A3, BD Sciences) or an isotype control (purified NA/LE mouse
182 $IgG_1κ$ Clone107.3, BD Sciences) for one hour at room temperature with gentle agitation before virus
183 infection or mock infection (43).
184
185 **Bioassay for antiviral activity.** Supernatants recovered from cells that were infected with MHV
186 strains at an MOI of 1 PFU/cell were exposed to 600 mJoules•cm^{-2} UVA light in a Stratalinker 1800
187 (Stratagene) to inactivate the virus. L2 mouse fibroblasts were treated with the UV-inactivated
188 supernatants for 24 hours and then infected with NDV-GFP at an MOI of 1 PFU/cell as described
189 previously (35). Control cells were treated with 100 U/mL universal IFNα (Quansys Biosciences, UT)
190 for 24 hours before NDV-GFP infection. At 12 and 24 hours post infection, cells were fixed in
191 Dulbecco's phosphate buffered saline (Gibco) containing 4% paraformaldehyde and examined for
192 enhanced-GFP (EGFP) expression under an Eclipse TE2000-U fluorescence microscope (Nikon

193 Instruments, Inc.). Images were acquired using NIS-Elements Basic Research microscope imaging
194 software (Nikon Instruments, Inc.).
195
196 **IFNβ quantification**. IFNβ protein in supernatants of MHV-infected BMM was quantified with a
197 commercial capture enzyme-linked immunosorbent assay kit (VeriKine Mouse Interferon Beta ELISA
198 Kit, PBL Laboratories, Piscataway, NJ) according to the manufacturer's instructions.
199
200 **Ribosomal RNA degradation assay.** For quantification of rRNA cleavage, total RNA from virus-
201 infected cells was isolated using an RNeasy kit (Qiagen) and quantified using a Nanodrop analyzer.
202 Equal amounts of RNA were separated on RNA chips and analyzed with an Agilent 2100
203 Bioanalyzer (Agilent Technologies) as described previously (25,44). RNA integrity numbers (referred
204 to as RIN values) (45) a measurement of RNA integrity produced by the bioanalyzer are also
205 indicated.
206
207 **Immunoblotting.** Cells were treated with 0 or 100 units/mL of universal IFNα, for four hours and
208 then lysed in nonidet P-40 (NP-40) buffer (1% NP-40, 2 mM EDTA, 10% glycerol, 150 mM NaCl and
209 50 mM Tris pH 8.0) containing protease inhibitors (Roche). Protein concentrations were measured
210 using a DC protein assay kit (Bio-Rad). Supernatants were mixed 1:1 with 2X SDS-PAGE sample
211 buffer. Samples were boiled, separated by 10% SDS-PAGE and transferred to polyvinylidene
212 difluoride (PVDF) membranes. Blots were blocked with 5% nonfat milk and probed with the following
213 antibodies directed against: OAS1A (clone E-2, Santa Cruz; 1:200), OAS2 (clone G-9, Santa Cruz,
214 1:200), OAS3 (clone D-7, Santa Cruz, 1:200), mouse RNase L (goat polyclonal T-16, Santa Cruz,
215 1:200), mouse RNase L (rabbit polyclonal; 1:1000) (46), human RNase L (mouse monoclonal
216 against human RNase L; 1:1000) (11) as well as anti-GAPDH-HRP (Abcam, 1:4000), anti-β-tubulin-
217 HRP (Abcam, 1:4000). Goat anti-mouse IgG_{2a}-HRP (Santa Cruz, 1:4000), goat anti-mouse HRP

218 (Santa Cruz; 1:5000), donkey anti-goat HRP (Santa Cruz; 1:5000) and donkey anti-rabbit IgG-HRP
219 (GE Healthcare, 1:10000) secondary antibodies were used to detect the primary antibodies of the
220 appropriate species. The blots were visualized using Super Signal West Dura Extended Duration
221 Substrate (Thermo Scientific). In Figures 4F and 5D blots were probed sequentially with antibodies
222 directed against OAS1, OAS2, OAS3, RNase L and GAPDH, with blots being stripped between
223 antibody treatments. In Figures 2D and 3B parallel gels were run and blotted with individual
224 antibodies. All immunoblots were performed at least twice.
225
226 **Quantifying IFNAR1 surface expression.** BMM and mixed glial cultures were stained with
227 antibodies against GFAP (BD, clone 1B4), CD11b (eBioscience, clone M1/70), F4/80 (Biolegend,
228 clone BM8), and the type I interferon receptor IFNAR1 (Biolegend, clone MAR1-5A3) or an isotype
229 control (Biolegend clone MOPC-21). Staining for GFAP was conducted following permeabilization
230 with the Cytofix/cytoperm Plus Fixation/Permeabilization kit (BD). Cells were analyzed with an LSR II
231 (Becton Dickinson) and resulting data was analyzed using FlowJo Software (Treestar). Astrocytes
232 ($GFAP^{+}CD11b^{-}F4/80^{-}$) and microglia ($GFAP^{-}CD11b^{+}F4/80^{+}$) from mixed cultures and macrophages
233 ($GFAP^{-}CD11b^{+}F4/80^{+}$) from bone marrow derived cultures were assessed for surface expression of
234 IFNAR1 (Biolegend, clone MAR1-5A3) or an isotype control (Biolegend clone MOPC-21).
235 Fluorescence intensity, dependent on both surface IFNAR1 density and cell surface area,
236 was normalized by cell size using previously described methods (47). This allowed us to compare
237 receptor density between cells of different sizes. Briefly, forward scatter (FSC), a measure of cell
238 volume, and side scatter (SSC), a measure of cell granularity, were used in a linear least-squares
239 regression model to determine fluorescence intensities corrected for cell size and shape. Residuals
240 from the model represent the variability in fluorescence that is not due to cell size and cell
241 granularity. These residuals were offset by the sample-specific average fluorescence intensity to
242 calculate the final values. Calculations and analysis were performed with MATLAB (Mathworks,
243 Natick, MD).

Statistical analysis. Plotting of data and statistical analysis were performed using GraphPad Prism software (GraphPad Software, Inc., CA) Statistical significance was determined by the unpaired two-tailed Student's t test.

RESULTS

Activation of RNase L during ns2^{H126R} infection of dendritic cells correlates with high basal *Oas* gene expression

We showed previously that while A59 antagonizes the OAS-RNase L pathway in myeloid lineage cells, including brain-resident microglia and liver-resident Kupffer cells as well as bone marrow derived macrophages (BMM) (2,25,29,34), ns2^{H126R}, a mutant expressing an inactive phosphodiesterase (PDE) fails to antagonize RNase L and consequently has severely restricted replication in these cell types. In contrast, replication of ns2^{H126R} in primary cell types including neurons, astrocytes, and hepatocytes as well as in immortalized cell lines was as robust as A59 (2,25,29). We investigated whether other myeloid cells, such as dendritic cells, would behave similarly to macrophages upon infection. Thus, we compared the replication of A59 and ns2^{H126R} in BMM and bone marrow derived dendritic cells (BMDC), derived from B6 (WT) mice. As observed in BMM (Figure 2A) (25,29), BMDC (Figure 2B) also restricted mutant virus replication by 100 fold at 12 hours ($p<0.01$) and 1000 fold after 24 hours post infection ($p<0.001$).

We next compared the basal level of expression of *Oas* genes in BMDC with those of BMM and neurons. Using real-time quantitative RT-PCR, we quantified basal levels of expression of three *Oas* genes that encode catalytically active OAS proteins, *Oas1a*, *Oas2*, and *Oas3*, in WT BMM and WT BMDC cultures in comparison to primary neurons (Figure 2C), the latter shown previously to express minimal basal levels of OAS genes and to be unable to restrict replication of ns2^{H126R} (29). *Oas* mRNA expression levels in neurons, as expected, were under the limit of detection and in comparison basal mRNA expression levels of Oas*1a*, *Oas2*, and *Oas3* genes in WT BMM and WT

270 BMDC were 1000 fold greater than the minimal detectable level (Figure 2C). Levels of OAS1A,
271 OAS2, OAS3 and RNase L were similar in BMM and BMDC culture, as assessed by immunoblotting
272 (Figure 2D). In order to compare RNase L activation during A59 and ns2^{H126R} infection, we monitored
273 the state of ribosomal RNA (rRNA) cleavage in WT BMM and BMDC infected with either ns2^{H126R} or
274 A59. The mutant virus ns2^{H126R} induced rRNA cleavage at 9 and 12 hours post infection in BMM and
275 BMDC (Figure 2E). In contrast, A59 did not induce rRNA cleavage, similar to mock infected cells,
276 even at the later time points. As a more quantitative measurement, RNA integrity numbers (referred
277 to as RIN values) (45) a measurement of RNA integrity produced by the bioanalyzer are also
278 indicated. Thus, BMDC behaved similarly to BMM in activation of RNase L and restriction of mutant
279 virus and activation of RNase L correlated with elevated basal levels of OAS genes (29).
280
281 **Overexpression of RNase L does not overcome low basal *Oas* mRNA expression to promote**
282 **RNase L activation by ns2^{H126R}**
283 We investigated whether the level of RNase L expression contributes to the differences
284 observed between activation of RNase L and ns2^{H126R} replication in myeloid and non-myeloid cells.
285 Thus, we compared BMM and astrocytes, the latter previously shown to express low levels of *Oas*
286 genes as compared with BMM (29). We quantified *Rnasel* protein levels by Western blot in BMM
287 and astrocytes using cells derived from *Rnasel*$^{-/-}$ mice as a negative control. RNase L protein
288 expression levels were similar in BMM and astrocytes (Figure 3A).
289 As RNase L activation is dependent on the production of 2-5A, we investigated whether
290 overexpression of RNase L might enable the low level of 2-5A produced by cells with low basal *Oas*
291 mRNA expression to activate RNase L to degrade rRNA in response to ns2^{H126R} infection. For this
292 we used a murine 3T3 cell line (3T3/pLZ) that stably overexpresses human RNase L from a
293 cytomegalovirus (CMV) promoter at a level greater than 100-fold that of endogenous murine RNase
294 L cells or endogenous human RNase L in A549 cell. Human RNase L was previously demonstrated
295 to be activated in 3T3/pLZ when exposed to 2-5A (33). Indeed, RNase L protein levels are much

296 greater in 3T3/pLZ cells as compared with A549 (Figure 3B). (The A549 cell line is derived from
297 human lung epithelium and expresses sufficient endogenous RNase L to be activated upon viral
298 infection (48).) However, the 3T3/pLZ cells and control 3T3/neo lacking the human RNase L gene
299 expressed a relatively low level of *Oas* mRNA similar to that of the murine L2 cell line (29) (Figure
300 3C). Upon infection of 3T3/pLZ cells with A59 and ns2^{H126R}, both viruses replicated to high titer as in
301 control 3T3/neo cells (Figure 3D). RNase L was not activated by ns2^{H126R}, as assessed by rRNA
302 degradation at 9 or 12 hours post infection (Figure 3E). However, treatment of 3T3/pLZ but not
303 3T3/neo with 2-5A activated RNase L demonstrating that human RNase L is indeed active in
304 3T3/pLZ cells. Thus, RNase L overexpression in 3T3/pLZ could not overcome the minimum 2-5A
305 threshold needed to activate RNase L.
306
307 **RNase L is activated in the absence of virus-induced interferon in macrophages**
308 While A59 induces type I IFN expression in only a limited number of cell types, primarily
309 myeloid cells (7,49), the activation of RNase L during infection (with ns2^{H126R}) occurs only in the
310 same limited cell types (7,29,49). Thus, we investigated whether virus-induced IFN was necessary
311 to activate RNase L presumably by further upregulating the already high basal levels of OAS
312 expression. IFN production during MHV infection of macrophages is dependent on MDA5 signaling
313 (7). Indeed, using a sensitive bioassay for antiviral activity (35) we confirmed that both A59 and
314 ns2^{H126R} infected WT BMM, secreted detectable antiviral activity at 12 and 24 hours post infection
315 (29), while infected MDA5 deficient (*Ifih1*$^{-/-}$) BMM failed to secrete detectable levels (Figure 4A). We
316 confirmed the presence of IFN in these WT BMM supernatants by quantifying the level of IFNβ
317 secreted at 12 hours post infection by ELISA. In WT BMM, MHV infection elicited detectable but low
318 levels (20 to 25 pg/mL) of IFNβ (Figure 4B), while *Ifih1*$^{-/-}$ BMM cultures did not produce detectable
319 IFNβ. Replication of ns2^{H126R} was 100 fold reduced at 12 hpi and 1000 fold attenuated after 24 hours

320 in *Ifih1*$^{-/-}$ macrophages (Figure 4D) compared to A59 in WT BMM (Figure 4C) (25) indicating that
321 ns2^{H126R} replication is restricted in BMM even in the absence of virus-induced IFN production.
322 Consistent with the above findings, we observed similar levels of *Oas* and *RnaseI* mRNA in
323 WT and *Ifih1*$^{-/-}$ BMM (Figure 4E). In addition, the corresponding protein levels of OAS1A, OAS2,
324 OAS3 and RNase L appeared to be at least as high in *Ifih1*$^{-/-}$ BMM as in WT BMM (Figure 4F). While
325 these immunoblot data show a small to modest increase in OAS1A, OAS2, OAS3 and RNase L
326 levels in *Ifih1*$^{-/-}$ cells compared to WT, other replicates failed to show any detectable differences
327 (data not shown). Furthermore, we compared the levels of other ISGs in WT and *Ifih1*$^{-/-}$ BMM and
328 found little difference in their relative mRNA expression levels, with the exception of MDA5, which as
329 expected was not expressed in *Ifih1*$^{-/-}$ BMM cultures (Figure 4G). Finally, RNase L activation was
330 observed in both genotypes of BMM by 12 hours post infection with ns2^{H126R} while it was also
331 evident at 9 hours in WT cells. Thus, infection with ns2^{H126R} activated RNase L in the absence of
332 virus-induced IFN (Figure 4H).
333
334 **Basal interferon signaling is required for maintenance of adequate *Oas* mRNA levels and**
335 **RNase L activation in macrophages**
336 Basal IFN signaling is necessary to maintain basal expression of ISGs, which enables the
337 cell to quickly respond to infection by inducing IFN as well as upregulating antiviral ISGs (50).
338 Indeed, we have reported much higher levels of ISG expression in myeloid cells that are able to
339 induce IFN and activate RNase L during MHV infection, as compared to other cell types (2,29). As in
340 the data shown above (Figure 4C), ns2^{H126R} was preferentially restricted compared to A59 in WT
341 BMM starting at 9 hours and 100-1000 fold decreased from 12 to 24 hours after infection (Figure
342 5A). However, replication of ns2^{H126R} was fully recovered in *Ifnar1*$^{-/-}$ BMM (Figure 5B).
343 We compared the expression of several *Oas* genes in WT and *Ifnar1*$^{-/-}$ BMM and found
344 reduced expression of *Oas1a* ($p<0.01$), *Oas2* ($p<0.001$), and *Oas3* ($p<0.01$) mRNAs in *Ifnar1*$^{-/-}$
345 BMM, presumably due to loss of basal IFN signaling, but no significant difference in *RnaseI* mRNA

346 expression (Figure 5C). Furthermore, we compared the basal protein expression levels of OAS1A,
347 OAS2, and RNase L in BMM derived from WT or *Ifnar1*$^{-/-}$ mice. OAS1A, OAS2 and OAS3 protein
348 was undetectable in cell lysates from *Ifnar1*$^{-/-}$ BMM cultures (Figure 5D) with or without prior IFN
349 treatment. While OAS proteins are modestly induced by IFN treatment of WT BMM, RNase L protein
350 expression is not dependent on IFNAR expression nor is it induced by IFN treatment. Basal
351 expression levels of other ISG mRNA [including *Ifih1* ($p<0.05$), *Ddx58* ($p<0.01$), *Ifit1, Ifit2*, *Isg15*, and
352 *Irf7* ($p<0.0001$)] were significantly decreased in the absence of IFNAR1 signaling compared to WT
353 BMM (Figure E). *Irf3* expression level, which is independent of IFNAR1 signaling (51), was similar in
354 WT and *Ifnar1*$^{-/-}$ BMM. Moreover, *Ifnb* expression levels were comparable in both genotypes and
355 near the limit of detection (Figure 5E). Additionally, degradation of rRNA was assessed in lysates
356 from infected BMM cultures at 9 and 12 hours post infection. In WT BMM cultures, ns2^{H126R} infection
357 induced rRNA degradation; however, in *Ifnar1*$^{-/-}$ BMM cultures, RNase L was not activated and rRNA
358 degradation was not observed (Figure 5F) supporting the notion that adequate basal levels of OAS
359 gene expression are required for activation of RNase L upon virus infection.

360 We hypothesized that the difference in basal ISG expression between macrophages and
361 astrocytes could be at least in part due to the cell surface expression level of type I interferon
362 receptor, IFNAR1. Cells with higher IFNAR1 surface expression might promote higher basal IFN
363 signaling and ISG levels and therefore be more likely to activate RNase L in the presence of dsRNA
364 early during ns2^{H126R} infection. To assess surface IFNAR1 expression on BMM, microglia and
365 astrocytes, BMM and primary astrocyte/microglia cultures were stained for identifying markers and
366 IFNAR1 and then analyzed by flow cytometry. As astrocytes displayed a larger range in size as
367 compared to macrophages (data not shown), we applied a size normalization algorithm to determine
368 density of surface IFNAR1. Using previously described methods (47) fluorescence intensity,
369 dependent on both surface IFNAR1 density and cell surface area, was normalized by cell size to
370 enable comparison of extent of relative IFNAR1 expression across cell types. Surface density of

371 IFNAR1 was higher in microglia and BMM compared to astrocytes (Figure 5G), perhaps
372 contributing to the higher extent of basal ISGs detected in myeloid cells.
373
374 **Modulation of surface IFNAR1 activity regulates basal *Oas* mRNA expression and RNase L**
375 **activation**
376 To complement the infections in *Ifnar1*$^{-/-}$ BMM and to further explore the relationship between
377 IFN signaling, basal *Oas* gene expression and activation of RNase L, we aimed to modulate IFNAR1
378 activity on WT BMM such that adequate basal IFN signaling would be maintained but the cells would
379 not be capable of further upregulating ISGs upon infection. We used a monoclonal antibody (MAR1-
380 5A3) specific for the IFNAR1 subunit of the murine IFN receptor that binds to cell surface IFNAR1
381 and blocks ligand-induced intracellular receptor signaling and induction of ISGs (37,52-54).
382 Following one hour of 2 µg/mL antibody pretreatment of WT BMM, there was no increase in *Oas*1,
383 *Oas*2 or *Oas*3 mRNA expression following infection, and the basal levels of mRNAs in mock infected
384 cells were the same as in "no mAb" controls (Figure 6A-C). Other ISGs, for example *Ifit1,* also failed
385 to be induced following infection (data not shown). Under these conditions, RNase L activity was still
386 activated by infection with ns2^{H126R} at 9 and 12 hours post infection (Figure 6G) resulting in
387 restriction of viral replication (Figure 6E). Thus, with a one hour pretreatment with 2 µg/mL of
388 antibody, basal mRNA levels of OAS genes are maintained and BMM retain the ability to restrict
389 MHV and activate RNase L, in the absence of upregulation of *Oas* expression levels. However, the
390 use of a higher dose of antibody (5 µg/mL) recapitulated the phenotype observed in *Ifnar1*$^{-/-}$ BMM in
391 that basal levels of *Oas* mRNA expression in mock infected mice were decreased approximately 10
392 fold (Figure 6A-C; compare mock infected, 5 µg/mL mAb treated to mock infected, no mAb
393 treatment). In addition, *Oas* mRNA levels were not induced by infection and activation of RNase L
394 did not occur as assessed by an rRNA degradation assay (Figure 6G) and replication of ns2^{H126R}
395 was no longer restricted (Figure 6F). It is important to note that treatment of cells with an isotype

396 control antibody had no effect on replication of A59 or ns2^{H126R} and that the replication of ns2^{H126R}
397 was restricted following treatment with isotype control antibody (Figure 6F) indicating the effects
398 were specific for IFNAR1 (Figures 6E&F). Thus, consistent with our observations from infection of
399 *Ifnar1*$^{-/-}$ and *Ifih1*$^{-/-}$ BMM (Figures 4&5) activation of RNase L correlated with *Oas* gene basal level of
400 expression and did not require further upregulation during infection.
401

402 **DISCUSSION**

403 OAS and RNase L comprise a potent antiviral pathway that is activated during viral infection
404 (13). The dsRNA generated during viral infection is sensed by several OAS proteins that respond by
405 synthesizing 2-5A that in turn induces the dimerization and activation of RNase L. RNase L
406 activation reduces viral replication and spread by degrading host and viral RNA limiting protein
407 synthesis and eventually leading to apoptosis (14). While the current paradigm is that upregulation
408 of OAS transcription by type I interferon during virus infection is needed to provide enough OAS
409 protein to activate the pathway, our data indicate that BMM are pre-armed with high basal levels of
410 OAS, sufficient to allow activation of RNase L upon sensing dsRNA early in infection. In addition to
411 BMM, brain-resident microglia (29), liver-resident Kupffer cells (data not shown) and BMDC (Figure
412 2) express high basal levels of OAS gene expression. Thus, in myeloid cells, RNase L activation
413 (right side of Figure 1) is not dependent on virus induction of IFN (the left side of Figure 1). This is
414 especially important when considering a virus like MHV that induce IFN only late in infection (49).
415 Conversely, in many non-myeloid cell types including primary hepatocytes, neurons, astrocytes and
416 murine cell lines, *Oas* expression levels are significantly lower. In these cells, ns2^{H126R} infection fails
417 to induce RNase L and MHV replicates to high titer, independent of ns2 PDE activity. These data
418 suggest that myeloid cells are able to quickly respond to early virus infection before IFN is induced,
419 thereby sparing non-renewable neighboring parenchymal cells from infection.

420 The correlation of RNase L activation with high basal *Oas* gene expression suggests that
421 production of 2-5A is the limiting step in activation. While *Oas* expression levels were quite variable
422 among murine cell types, we found similar levels of RNase L expression in murine BMM and
423 astrocytes (Figure 3A), cell types expressing high and low levels of *Oas* genes, respectively.
424 Furthermore basal levels of *RNasel* transcripts and proteins were not dependent on IFNAR signaling
425 in BMM (Figure 5C&5D). However, to investigate whether a high level of RNase L could overcome
426 the requirement for high OAS levels to produce 2-5A, we carried out infections in murine 3T3/pLZ
427 cells, which overexpress RNase L to a level about 100 fold greater than endogenous RNase L (33).
428 Since MHV induces type I IFN in myeloid cells only and not mouse fibroblast cell lines, RNase L
429 activation depends on basal OAS expression levels and RNase L was not activated in this cell type
430 by either A59 or ns2^{H126R} while treatment with 2-5A directly activated RNase L and promoted RNA
431 degradation in 3T3/pLZ but not 3T3/neo cells (Figure 3E). These findings indicate that OAS activity
432 is the limiting step for RNase L activation during infection, as extremely high levels of RNase L were
433 not sufficient to overcome insufficient levels of *Oas* gene expression.

434 We present further evidence that in myeloid cells, RNase L can be activated in the absence
435 of MDA5, the recognition receptor necessary for the induction of IFN during MHV infection (7), as
436 long as *Oas* gene expression remains at an adequate level. However, we did observe delays in both
437 RNase L activation and restriction of ns2^{H126R} replication in *Ifih1*$^{-/-}$ as compared with B6 BMM (Fig
438 4C&D,H; compare 9 and 12 hour points), suggesting that the induction of IFN during infection in B6
439 BMM may accelerate the activation of RNase L. The reduced levels of *Oas* gene expression in BMM
440 derived from *Ifnar1*$^{-/-}$ mice or B6 mice treated with 5 µg/mL IFNAR1 blocking antibody preclude the
441 activation of RNase L during ns2^{H126R} infection. These data suggest that the basal level of *Oas*
442 expressed in BMM derived from WT B6 or *Ifih1*$^{-/-}$ mice is both necessary and adequate to produce
443 enough 2-5A to activate RNase L in the absence of virus-induced IFN.

444 IFN is vital for control of early MHV infection *in vivo* (6-8). However, MHV and other
445 coronaviruses, such as severe acute respiratory syndrome coronavirus (SARS-CoV) and Middle

East respiratory syndrome coronavirus (MERS-CoV) are poor inducers of IFN as they actively avoid and/or inhibit a robust type I IFN response in infected cells (49,55-60). In the case of MHV, IFN is not detected during infection of cell lines nor in several types of primary cells *in vitro*, including the main types of cells infected in the major targets of infection, the brain (neurons, astrocytes, and oligodendrocytes) and the liver (hepatocytes). However, MHV does induce IFN in macrophages and microglia in the brain (7) as well as pDCs *in vivo* (17) and in myeloid cells *in vitro* (7). These are the same types of cells expressing high levels of basal *Oas* genes and which activate RNase L in response to ns2^{H126R}, probably as a consequence of the high expression levels of ISGs including MDA5 and the transcription factors necessary for IFN induction (2,29). Thus, *in vivo,* low *Oas* gene expressing cells may be induced by paracrine IFN to increase OAS levels enabling viral activation of RNase L. Indeed, in previous experiments reported by our lab, pretreatment of astrocyte or neurons with IFN did increase the levels of *Oas* gene expression (29). However, IFN pretreatment also resulted in decreased titers of both A59 and ns2^{H126R} and the absence of activation of RNase L in those experiments was suggested to be a consequence of reduced ability of both A59 and ns2^{H126R} to replicate and produce dsRNA following IFN pretreatment (29). We infer from these data that, not surprisingly, IFN treatment induces many antiviral ISGs some of which inhibit viral replication without the activation of RNase L. Furthermore, high basal *Oas* levels are necessary for the activation of RNase L by MHV lacking a functional viral PDE.

Type I IFNs are produced constitutively in very low quantities, barely detectable at the mRNA and protein levels in some cell types, such as BMM cultures (Figure 5E, data not shown), and undetectable in most other cell types we have tested (data not shown). However, this low level of constitutive IFN is believed to have many important effects for the host including cytokine induction, immune cell activity, maintenance and mobilization of hematopoietic stem cells and antitumor effects (50,61). In addition, and most relevant to this work, constitutive IFN signaling is important for maintaining adequate basal levels of ISGs to promote rapid and efficient responses to microbial invasion as evidenced by the extreme sensitivity of *Ifnar1*$^{-/-}$ mice to many viruses, including MHV. It

472 is important that the levels of constitutive IFN be carefully regulated as excessive IFN can have
473 pathological effects, contributing to several autoimmune diseases and promoting cancer (50,61,62).
474 Little is known about the regulation of secretion or activity of constitutive IFN. While the
475 transcriptional regulation of IFNβ following viral infection has been extensively characterized, less is
476 known regarding the transcriptional regulation of constitutive basal IFNβ expression. However, it is
477 known that constitutive IFN production is dependent on IRF-3 and IRF-7, two major transcription
478 factors driving type I IFN transcription following viral infection (51,63), but repressed by IRF-2, which
479 binds to the IFNβ promoter and contributes to tight control of basal expression (64,65)., We found
480 that astrocytes have a significantly higher basal *Irf2* mRNA expression level than BMM (data not
481 shown).
482 There is some evidence that IFNAR1 expression level may play a role in viral pathogenesis,
483 in that it was recently reported that the encephalitic flaviviruses, tick-borne encephalitis virus and
484 West Nile virus, antagonize IFN signaling by downregulating IFNAR1 surface expression thus
485 reducing IFNβ-stimulated antiviral gene induction and compromising host control of infection (66).
486 Interestingly, in a reovirus model of myocarditis, surface expression levels of IFNAR as well as basal
487 ISG levels were higher in cardiac fibroblasts as compared with cardiac myocytes. It was suggested
488 that upon exposure to IFN cardiac fibroblasts could quickly develop an antiviral state and thereby
489 avoid serving as a site of replication and spread to the non-renewable cardiac myocytes (67).
490 Similarly our data suggest that astrocytes have relatively lower IFNAR1 surface expression
491 compared to microglia in the brain or BMM (Figure 5G), which could contribute to the lower level of
492 basal ISG expression. We found that astrocytes and neurons did not activate RNase L activity in
493 response to a variety of viruses including MHV, encephalomyocarditis virus, Sendai virus, and
494 LaCrosse virus (29), likely a consequence of low basal ISG expression. Terminally differentiated
495 astrocytes and neurons might have limited IFN responsiveness and secretion to prevent damage to

496 the CNS. This is in contrast to renewable myeloid cells such as macrophages and microglia that are
497 primed to respond to viral infection and reduce viral spread to other cell types.

498 As described above, we have found that activation of RNase L correlates with high basal
499 *Oas* mRNA expression in analysis of myeloid versus non-myeloid cell types, in B6 versus *Ifih1*$^{-/-}$ and
500 Ifnar1$^{-/-}$ BMM and in the cells treated with antibody to IFNAR1 versus untreated controls. Basal
501 expression of OAS1a, OAS2 and OAS3 proteins were dependent on IFNAR expression and levels in
502 myeloid cells were sufficient to activate RNase L upon viral infection. There are little if any data
503 indicating which *Oas* genes are most important for RNase L activation in response to viral infections.
504 Future work is being conducted to determine the role of individual *Oas* genes in activating RNase L.

505

506

507

508 **ACKNOWLEDGEMENTS**

509 This work was supported by NIH grants R01-NS081008 and R01-NS054695 (SRW), R01-AI104887
510 (SRW and RHS) and R01-CA044059 (RHS). LDB and KMR were each supported in part by training
511 grant T32-AI007324 and ZBZ was supported in part by T32-NS-007180. We are grateful to Dr.
512 Babal Jha (Cleveland Clinic) for the HPLC purified 2-5A.

513 **REFERENCES**

514 1. **Navas-Martin S, Weiss SR.** 2003. SARS: lessons learned from other coronaviruses. Viral
515 Immunol **16:**461-474.
516 2. **Zhao L, Rose KM, Elliott R, Van Rooijen N, Weiss SR.** 2011. Cell-type-specific type I
517 interferon antagonism influences organ tropism of murine coronavirus. Journal of virology
518 **85:**10058-10068.
519 3. **Lavi E, Gilden DH, Wroblewska Z, Rorke LB, Weiss SR.** 1984. Experimental
520 demyelination produced by the A59 strain of mouse hepatitis virus. Neurology **34:**597-603.
521 4. **Marten NW, Stohlman SA, Atkinson RD, Hinton DR, Fleming JO, Bergmann CC.** 2000.
522 Contributions of CD8+ T cells and viral spread to demyelinating disease. J Immunol
523 **164:**4080-4088.
524 5. **Marten NW, Stohlman SA, Bergmann CC.** 2001. MHV infection of the CNS: mechanisms of
525 immune-mediated control. Viral Immunol 2001;14(1):1-18 **14:**1-18.
526 6. **Ireland DD, Stohlman SA, Hinton DR, Atkinson R, Bergmann CC.** 2008. Type I
527 interferons are essential in controlling neurotropic coronavirus infection irrespective of
528 functional CD8 T cells. J Virol **82:**300-310.
529 7. **Roth-Cross JK, Bender SJ, Weiss SR.** 2008. Murine coronavirus mouse hepatitis virus is
530 recognized by MDA5 and induces type I interferon in brain macrophages/microglia. J Virol
531 **82:**9829-9838.
532 8. **Cervantes-Barragan L, Zust R, Weber F, Spiegel M, Lang KS, Akira S, Thiel V, Ludewig**
533 **B.** 2007. Control of coronavirus infection through plasmacytoid dendritic-cell-derived type I
534 interferon. Blood **109:**1131-1137.
535 9. **Kumagai Y, Takeuchi O, Akira S.** 2008. Pathogen recognition by innate receptors. J Infect
536 Chemother **14:**86-92.
537 10. **Takeuchi O, Akira S.** 2007. Recognition of viruses by innate immunity. Immunol Rev
538 **220:**214-224.
539 11. **Dong B, Silverman RH.** 1995. 2-5A-dependent RNase molecules dimerize during activation
540 by 2-5A. J Biol Chem **270:**4133-4137.
541 12. **Malathi K, Dong B, Gale M, Jr., Silverman RH.** 2007. Small self-RNA generated by RNase
542 L amplifies antiviral innate immunity. Nature **448:**816-819.
543 13. **Silverman RH.** 2007. Viral encounters with 2',5'-oligoadenylate synthetase and RNase L
544 during the interferon antiviral response. J Virol **81:**12720-12729.
545 14. **Zhou A, Paranjape J, Brown TL, Nie H, Naik S, Dong B, Chang A, Trapp B, Fairchild R,**
546 **Colmenares C, Silverman RH.** 1997. Interferon action and apoptosis are defective in mice
547 devoid of 2',5'-oligoadenylate-dependent RNase L. EMBO J **16:**6355-6363.
548 15. **Durbin JE, Fernandez-Sesma A, Lee CK, Rao TD, Frey AB, Moran TM, Vukmanovic S,**
549 **Garcia-Sastre A, Levy DE.** 2000. Type I IFN modulates innate and specific antiviral
550 immunity. J Immunol **164:**4220-4228.
551 16. **Muller U, Steinhoff U, Reis LF, Hemmi S, Pavlovic J, Zinkernagel RM, Aguet M.** 1994.
552 Functional role of type I and type II interferons in antiviral defense. Science **264:**1918-1921.
553 17. **Cervantes-Barragan L, Lewis KL, Firner S, Thiel V, Hugues S, Reith W, Ludewig B,**
554 **Reizis B.** 2012. Plasmacytoid dendritic cells control T-cell response to chronic viral infection.
555 Proc Natl Acad Sci U S A **109:**3012-3017.
556 18. **Silverman RH.** 2007. A scientific journey through the 2-5A/RNase L system. Cytokine
557 Growth Factor Rev **18:**381-388.
558 19. **Kakuta S, Shibata S, Iwakura Y.** 2002. Genomic structure of the mouse 2',5'-oligoadenylate
559 synthetase gene family. J Interferon Cytokine Res **22:**981-993.
560 20. **Mashimo T, Glaser P, Lucas M, Simon-Chazottes D, Ceccaldi PE, Montagutelli X,**
561 **Despres P, Guenet JL.** 2003. Structural and functional genomics and evolutionary
562 relationships in the cluster of genes encoding murine 2',5'-oligoadenylate synthetases.
563 Genomics **82:**537-552.

564 21. **Silverman RH, Weiss SR.** 2014. Viral phosphodiesterases that antagonize double-stranded
565 RNA signaling to RNase L by degrading 2-5A. J Interferon Cytokine Res **34:**455-463.
566 22. **Stark GR, Kerr IM, Williams BR, Silverman RH, Schreiber RD.** 1998. How cells respond to
567 interferons. Annu Rev Biochem **67:**227-264.
568 23. **Castelli J, Wood KA, Youle RJ.** 1998. The 2-5A system in viral infection and apoptosis.
569 Biomed Pharmacother **52:**386-390.
570 24. **Castelli JC, Hassel BA, Maran A, Paranjape J, Hewitt JA, Li XL, Hsu YT, Silverman RH,**
571 **Youle RJ.** 1998. The role of 2'-5' oligoadenylate-activated ribonuclease L in apoptosis. Cell
572 Death Differ **5:**313-320.
573 25. **Zhao L, Jha BK, Wu A, Elliott R, Ziebuhr J, Gorbalenya AE, Silverman RH, Weiss SR.**
574 2012. Antagonism of the interferon-induced OAS-RNase L pathway by murine coronavirus
575 ns2 protein is required for virus replication and liver pathology. Cell Host & Microbe **11:**607-
576 616.
577 26. **Sorgeloos F, Jha BK, Silverman RH, Michiels T.** 2013. Evasion of antiviral innate
578 immunity by Theiler's virus L* protein through direct inhibition of RNase L. PLoS Pathog
579 **9:**e1003474.
580 27. **Randall RE, Goodbourn S.** 2008. Interferons and viruses: an interplay between induction,
581 signalling, antiviral responses and virus countermeasures. J Gen Virol **89:**1-47.
582 28. **Han JQ, Townsend HL, Jha BK, Paranjape JM, Silverman RH, Barton DJ.** 2007. A
583 phylogenetically conserved RNA structure in the poliovirus open reading frame inhibits the
584 antiviral endoribonuclease RNase L. J Virol **81:**5561-5572.
585 29. **Zhao L, Birdwell LD, Wu A, Elliott R, Rose KM, Phillips JM, Li Y, Grinspan J, Silverman**
586 **RH, Weiss SR.** 2013. Cell-type-specific activation of the oligoadenylate synthetase-RNase L
587 pathway by a murine coronavirus. J Virol **87:**8408-8418.
588 30. **Taniguchi T, Takaoka A.** 2001. A weak signal for strong responses: interferon-alpha/beta
589 revisited. Nat Rev Mol Cell Biol **2:**378-386.
590 31. **Sato M, Taniguchi T, Tanaka N.** 2001. The interferon system and interferon regulatory
591 factor transcription factors -- studies from gene knockout mice. Cytokine Growth Factor Rev
592 **12:**133-142.
593 32. **Gombold JL, Hingley ST, Weiss SR.** 1993. Fusion-defective mutants of mouse hepatitis
594 virus A59 contain a mutation in the spike protein cleavage signal. J Virol **67:**4504-4512.
595 33. **Zhou A, Paranjape JM, Hassel BA, Nie H, Shah S, Galinski B, Silverman RH.** 1998.
596 Impact of RNase L overexpression on viral and cellular growth and death. J Interferon
597 Cytokine Res **18:**953-961.
598 34. **Roth-Cross JK, Stokes H, Chang G, Chua MM, Thiel V, Weiss SR, Gorbalenya AE,**
599 **Siddell SG.** 2009. Organ-specific attenuation of murine hepatitis virus strain A59 by
600 replacement of catalytic residues in the putative viral cyclic phosphodiesterase ns2. J Virol
601 **83:**3743-3753.
602 35. **Park MS, Shaw ML, Munoz-Jordan J, Cros JF, Nakaya T, Bouvier N, Palese P, Garcia-**
603 **Sastre A, Basler CF.** 2003. Newcastle disease virus (NDV)-based assay demonstrates
604 interferon-antagonist activity for the NDV V protein and the Nipah virus V, W, and C proteins.
605 J Virol **77:**1501-1511.
606 36. **Gitlin L, Barchet W, Gilfillan S, Cella M, Beutler B, Flavell RA, Diamond MS, Colonna M.**
607 2006. Essential role of mda-5 in type I IFN responses to polyriboinosinic:polyribocytidylic acid
608 and encephalomyocarditis picornavirus. Proc Natl Acad Sci U S A **103:**8459-8464.
609 37. **Pinto AK, Daffis S, Brien JD, Gainey MD, Yokoyama WM, Sheehan KC, Murphy KM,**
610 **Schreiber RD, Diamond MS.** 2011. A temporal role of type I interferon signaling in CD8+ T
611 cell maturation during acute West Nile virus infection. PLoS Pathog **7:**e1002407.
612 38. **Casson CN, Copenhaver AM, Zwack EE, Nguyen HT, Strowig T, Javdan B, Bradley WP,**
613 **Fung TC, Flavell RA, Brodsky IE, Shin S.** 2013. Caspase-11 activation in response to
614 bacterial secretion systems that access the host cytosol. PLoS Pathog **9:**e1003400.

Journal of Virology

615 39. **Caamano J, Alexander J, Craig L, Bravo R, Hunter CA.** 1999. The NF-kappa B family
616 member RelB is required for innate and adaptive immunity to Toxoplasma gondii. J Immunol
617 **163:**4453-4461.
618 40. **Inaba K, Inaba M, Romani N, Aya H, Deguchi M, Ikehara S, Muramatsu S, Steinman RM.**
619 1992. Generation of large numbers of dendritic cells from mouse bone marrow cultures
620 supplemented with granulocyte/macrophage colony-stimulating factor. J Exp Med **176:**1693-
621 1702.
622 41. **Copenhaver AM, Casson CN, Nguyen HT, Fung TC, Duda MM, Roy CR, Shin S.** 2014.
623 Alveolar macrophages and neutrophils are the primary reservoirs for Legionella pneumophila
624 and mediate cytosolic surveillance of type IV secretion. Infect Immun **82:**4325-4336.
625 42. **Bender SJ, Phillips JM, Scott EP, Weiss SR.** 2010. Murine coronavirus receptors are
626 differentially expressed in the central nervous system and play virus strain-dependent roles
627 in neuronal spread. J Virol **84:**11030-11044.
628 43. **Sheehan KC, Lai KS, Dunn GP, Bruce AT, Diamond MS, Heutel JD, Dungo-Arthur C,**
629 **Carrero JA, White JM, Hertzog PJ, Schreiber RD.** 2006. Blocking monoclonal antibodies
630 specific for mouse IFN-alpha/beta receptor subunit 1 (IFNAR-1) from mice immunized by in
631 vivo hydrodynamic transfection. J Interferon Cytokine Res **26:**804-819.
632 44. **Xiang Y, Wang Z, Murakami J, Plummer S, Klein EA, Carpten JD, Trent JM, Isaacs WB,**
633 **Casey G, Silverman RH.** 2003. Effects of RNase L mutations associated with prostate
634 cancer on apoptosis induced by 2',5'-oligoadenylates. Cancer Res **63:**6795-6801.
635 45. **Schroeder A, Mueller O, Stocker S, Salowsky R, Leiber M, Gassmann M, Lightfoot S,**
636 **Menzel W, Granzow M, Ragg T.** 2006. The RIN: an RNA integrity number for assigning
637 integrity values to RNA measurements. BMC Mol Biol **7:**3.
638 46. **Zhou Y, Kang MJ, Jha BK, Silverman RH, Lee CG, Elias JA.** 2013. Role of ribonuclease L
639 in viral pathogen-associated molecular pattern/influenza virus and cigarette smoke-induced
640 inflammation and remodeling. J Immunol **191:**2637-2646.
641 47. **Knijnenburg TA, Roda O, Wan Y, Nolan GP, Aitchison JD, Shmulevich I.** 2011. A
642 regression model approach to enable cell morphology correction in high-throughput flow
643 cytometry. Mol Syst Biol **7:**531.
644 48. **Cooper DA, Banerjee S, Chakrabarti A, Garcia-Sastre A, Hesselberth JR, Silverman**
645 **RH, Barton DJ.** 2015. RNase L targets distinct sites in influenza A virus RNAs. J Virol
646 **89:**2764-2776.
647 49. **Roth-Cross JK, Martinez-Sobrido L, Scott EP, Garcia-Sastre A, Weiss SR.** 2007.
648 Inhibition of the alpha/beta interferon response by mouse hepatitis virus at multiple levels. J
649 Virol **81:**7189-7199.
650 50. **Gough DJ, Messina NL, Clarke CJ, Johnstone RW, Levy DE.** 2012. Constitutive type I
651 interferon modulates homeostatic balance through tonic signaling. Immunity **36:**166-174.
652 51. **Sato M, Suemori H, Hata N, Asagiri M, Ogasawara K, Nakao K, Nakaya T, Katsuki M,**
653 **Noguchi S, Tanaka N, Taniguchi T.** 2000. Distinct and essential roles of transcription
654 factors IRF-3 and IRF-7 in response to viruses for IFN-alpha/beta gene induction. Immunity
655 **13:**539-548.
656 52. **Lazear HM, Pinto AK, Vogt MR, Gale M, Jr., Diamond MS.** 2011. Beta interferon controls
657 West Nile virus infection and pathogenesis in mice. Journal of virology **85:**7186-7194.
658 53. **Fenner JE, Starr R, Cornish AL, Zhang JG, Metcalf D, Schreiber RD, Sheehan K, Hilton**
659 **DJ, Alexander WS, Hertzog PJ.** 2006. Suppressor of cytokine signaling 1 regulates the
660 immune response to infection by a unique inhibition of type I interferon activity. Nat Immunol
661 **7:**33-39.
662 54. **Samuel MA, Whitby K, Keller BC, Marri A, Barchet W, Williams BR, Silverman RH, Gale**
663 **M, Jr., Diamond MS.** 2006. PKR and RNase L contribute to protection against lethal West
664 Nile Virus infection by controlling early viral spread in the periphery and replication in
665 neurons. J Virol **80:**7009-7019.

55. **Chan RW, Chan MC, Agnihothram S, Chan LL, Kuok DI, Fong JH, Guan Y, Poon LL, Baric RS, Nicholls JM, Peiris JS.** 2013. Tropism of and innate immune responses to the novel human betacoronavirus lineage C virus in human ex vivo respiratory organ cultures. J Virol **87:**6604-6614.
56. **Spiegel M, Pichlmair A, Martinez-Sobrido L, Cros J, Garcia-Sastre A, Haller O, Weber F.** 2005. Inhibition of Beta interferon induction by severe acute respiratory syndrome coronavirus suggests a two-step model for activation of interferon regulatory factor 3. J Virol **79:**2079-2086.
57. **Versteeg GA, Bredenbeek PJ, van den Worm SH, Spaan WJ.** 2007. Group 2 coronaviruses prevent immediate early interferon induction by protection of viral RNA from host cell recognition. Virology **361:**18-26.
58. **Kindler E, Jonsdottir HR, Muth D, Hamming OJ, Hartmann R, Rodriguez R, Geffers R, Fouchier RA, Drosten C, Muller MA, Dijkman R, Thiel V.** 2013. Efficient replication of the novel human betacoronavirus EMC on primary human epithelium highlights its zoonotic potential. MBio **4:**e00611-00612.
59. **Chan JF, Chan KH, Choi GK, To KK, Tse H, Cai JP, Yeung ML, Cheng VC, Chen H, Che XY, Lau SK, Woo PC, Yuen KY.** 2013. Differential cell line susceptibility to the emerging novel human betacoronavirus 2c EMC/2012: implications for disease pathogenesis and clinical manifestation. J Infect Dis **207:**1743-1752.
60. **Zielecki F, Weber M, Eickmann M, Spiegelberg L, Zaki AM, Matrosovich M, Becker S, Weber F.** 2013. Human cell tropism and innate immune system interactions of human respiratory coronavirus EMC compared to those of severe acute respiratory syndrome coronavirus. J Virol **87:**5300-5304.
61. **Trinchieri G.** 2010. Type I interferon: friend or foe? J Exp Med **207:**2053-2063.
62. **de Visser KE, Eichten A, Coussens LM.** 2006. Paradoxical roles of the immune system during cancer development. Nat Rev Cancer **6:**24-37.
63. **Hata N, Sato M, Takaoka A, Asagiri M, Tanaka N, Taniguchi T.** 2001. Constitutive IFN-alpha/beta signal for efficient IFN-alpha/beta gene induction by virus. Biochem Biophys Res Commun **285:**518-525.
64. **Harada H, Fujita T, Miyamoto M, Kimura Y, Maruyama M, Furia A, Miyata T, Taniguchi T.** 1989. Structurally similar but functionally distinct factors, IRF-1 and IRF-2, bind to the same regulatory elements of IFN and IFN-inducible genes. Cell **58:**729-739.
65. **Taniguchi T, Ogasawara K, Takaoka A, Tanaka N.** 2001. IRF family of transcription factors as regulators of host defense. Annu Rev Immunol **19:**623-655.
66. **Lubick KJ, Robertson SJ, McNally KL, Freedman BA, Rasmussen AL, Taylor RT, Walts AD, Tsuruda S, Sakai M, Ishizuka M, Boer EF, Foster EC, Chiramel AI, Addison CB, Green R, Kastner DL, Katze MG, Holland SM, Forlino A, Freeman AF, Boehm M, Yoshii K, Best SM.** 2015. Flavivirus Antagonism of Type I Interferon Signaling Reveals Prolidase as a Regulator of IFNAR1 Surface Expression. Cell Host Microbe **18:**61-74.
67. **Zurney J, Howard KE, Sherry B.** 2007. Basal expression levels of IFNAR and Jak-STAT components are determinants of cell-type-specific differences in cardiac antiviral responses. J Virol **81:**13668-13680.

713

714

715

716

717

718

719 **FIGURE LEGENDS**

720 **Figure 1. OAS-RNase L pathway. Interferon induction and signaling (left side). (1)** Viral dsRNA
721 is produced during virus replication and **(2)** sensed by PRRs such as MDA5, initiating a signaling
722 pathway leading to **(3)** transcription, translation and secretion of IFNα/β. **(4)** Autocrine and paracrine
723 IFN signaling through the interferon receptor (IFNAR1) **(5,6)** stimulates the expression of ISGs.
724 **RNase L activation (right side). (7)** OASs sense viral dsRNA and synthesize 2-5A. **(8)** 2-5A binds
725 to RNase L inducing its dimerization and subsequent activation. **(9)** RNase L degrades RNA.

726

727 **Figure 2. Activation of RNase L by ns2^{H126R} during infection of BMM and BMDC cultures. (A)**
728 BMM and **(B)** BMDC cultures were infected with A59 or ns2^{H126R} (1 PFU/cell) and at the times
729 indicated, the virus titer was determined by plaque assay from the supernatant. The data are pooled
730 from two independent experiments carried out in triplicate and shown as the means ± SEM. *, P<
731 0.05; **, P < 0.01; ***, P < 0.001. **(C)** RNA was extracted from infected BMM, BMDC and neuron
732 cultures and *Oas1a*, *Oas2*, and *Oas3* mRNA expression was quantified by qRT-PCR. mRNA
733 expression levels relative to β-actin mRNA are expressed as $2^{-\Delta C_T}$, where $\Delta C_T = (C_{T,\ \text{Target Gene}} - C_{T,\ \beta\text{-}$
734 $\text{actin}})$. The dashed line designates the lower limit of detection. These data are from one representative
735 experiment of two, each performed in triplicate. **(D)** Protein lysates from BMM and BMDC were
736 electrophoresed in acrylamide gels and then probed with antibodies against OAS1A, OAS2, OAS3,
737 RNase L (mAb) and GAPDH. **(E)** RNA was extracted from infected BMM and BMDC cultures at 9
738 and 12 hours post infection as well as cultures 12 hours post mock infection and rRNA degradation
739 was assessed with a Bioanalyzer. RNA integrity numbers (referred to as RIN values) (45) a
740 measurement of RNA integrity produced by the bioanalyzer are also indicated. The positions of 28S
741 and 18S rRNAs are indicated.

742

743 **Figure 3. Overexpression of RNase L is not sufficient to overcome low OAS levels to promote**
744 **RNase L degradation**. **(A)** Proteins were extracted from WT and *Rnasel*$^{-/-}$ BMM and astrocytes,

745 electrophoresed in polyacrylamide gels and probed by Western blot with antibodies directed against
746 RNase L (rabbit polyclonal) and β-tubulin. BMM and astrocyte cell lysates were electrophoresed on
747 the same gel and blot; intervening lanes were removed and replaced by space between samples.
748 **(B)** Proteins were extracted from human A549 and murine 3T3/pLZ cells, electrophoresed in
749 polyacrylamide gels and probed by Western blot with antibodies directed against human RNase L
750 and human β-tubulin. **(C)** RNA was extracted from L2, 3T3/pLZ, 3T3/neo and BMM cultures and
751 basal expression levels of *Oas* mRNAs were quantified by qRT-PCR. mRNA expression levels
752 relative to β-actin mRNA are expressed as $2^{-\Delta CT}$, where $\Delta C_T = (C_{T,\ \text{Target Gene}} - C_{T,\ \beta\text{-actin}})$. Data are from
753 one representative experiment of two (except for pLZ/neo mRNA) each performed in triplicate. The
754 dashed line designates the lower limit of detection. **(D)** 3T3/pLZ and 3T3/neo cells were infected with
755 A59 or ns2^{H126R} (1 PFU/cell) and at the times indicated, the virus titer was determined by plaque
756 assay from the supernatant. Data are pooled from two independent experiments (3T3/pLZ) or from
757 one experiment (3T3/neo) each performed in triplicate. **(E)** 3T3/pLZ and 3T3/neo cells were mock
758 infected or infected with A59 or ns2^{H126R} (1 PFU/cell) and at 12 hours post infection, cells were lysed
759 and RNA extracted. In a separate experiment cells were transfected with 10 μM 2-5A in
760 Lipofectamine, with Lipofectamine alone or left untreated and 4 hours later cells were lysed and
761 RNA extracted. rRNA degradation was assessed with a Bioanalyzer. 28S and 18S rRNAs are
762 indicated.
763
764 **Figure 4. Infection of *Ifih1*$^{-/-}$ macrophages with A59 and ns2^{H126R}. (A)** WT or *Ifih1*$^{-/-}$ BMM cultures
765 were either mock infected or infected with A59 or ns2^{H126R} (1 PFU/cell). At 12 hours post infection,
766 supernatants were treated with UV light to inactivate virus and incubated with L2 mouse fibroblasts
767 for 24 h, followed by infection with NDV-GFP (1 PFU/cell). As a positive control, L2 cells were
768 treated with IFNα for 24 h and then infected with NDV-GFP. At 12 or 24 hours post infection, cells
769 were fixed and examined for enhanced-GFP expression by microscopy. The white lines represent
770 50 μm. **(B)** Supernatants taken at 12 hours post infection from the same mock infected or A59 and

771 ns2^{H126R} infected WT and *Ifih1*$^{-/-}$ BMM cultures were analyzed by ELISA for mouse IFNβ by VeriKine
772 kit. Limit of detection is indicated by dashed line. Data are from one representative experiment of
773 two. **(C)** WT BMM and **(D)** *Ifih1*$^{-/-}$ BMM cultures were infected with A59 and ns2^{H126R} (1 PFU/cell) and
774 at the times indicated, the virus titer was determined by plaque assay from the supernatant. Data are
775 pooled from two independent experiments performed in triplicate and shown as the means ± SEM. *,
776 P < 0.05; **, P < 0.01; ***, P< 0.001. **(E and G)** mRNA expression levels relative to β-actin mRNA
777 are expressed as $2^{-\Delta C_T}$, where $\Delta C_T = (C_{T,\ \text{Target Gene}} - C_{T,\ \beta\text{-actin}})$. Dashed line designates the lower limit
778 of detection. Data shown are pooled from two independent experiments each performed in triplicate
779 and shown as the means ± SEM. *, P < 0.05; **, P < 0.01; ***, P< 0.001. **(F)** Proteins were extracted
780 from WT and *Ifih1*$^{-/-}$ BMM and probed by Western blot with antibodies directed against OAS1A,
781 OAS2, OAS3, RNase L (mAb) and GAPDH. **(H)** RNA was extracted from infected WT and *Ifih1*$^{-/-}$
782 BMM cultures at 9 and 12 hours post infection as well as cultures 12 hours post mock infection and
783 rRNA degradation was assessed with a Bioanalyzer. 28S and 18S rRNAs are indicated.
784
785 **Figure 5. RNase L is not activated during infection of *Ifnar1*$^{-/-}$ macrophages. (A)** WT and **(B)**
786 *Ifnar1*$^{-/-}$ BMM cultures were infected with A59 or ns2^{H126R} (1 PFU/cell) and at times indicated virus
787 titered by plaque assay from the supernatant. Data are pooled from two independent experiments
788 performed in triplicate and shown as the means ± SEM. *, P < 0.05; **, P < 0.01. **(C)** RNA was
789 extracted from uninfected WT and *Ifnar1*$^{-/-}$ BMM cultures and *Oas1a, Oas2, Oas3, and Rnasel*
790 mRNA were quantified by qRT-PCR. mRNA expression levels relative to β-actin mRNA are
791 expressed as $2^{-\Delta CT}$, where $\Delta C_T = (C_{T,\ \text{Target Gene}} - C_{T,\ \beta\text{-actin}})$. The dashed line designates the lower limit
792 of detection. Data are pooled from two independent experiments, each performed in triplicate and
793 shown as the means ± SEM. **, P < 0.01; ***, P< 0.001. **(D)** WT and *Ifnar1*$^{-/-}$ BMM cultures were
794 either mock treated or treated with 100 U/mL of universal IFNα for four hours; protein was extracted
795 and electrophoresed in polyacrylamide gels and probed with antibodies directed against OAS1A,

796 OAS2, OAS3, RNase L (mAb) and GAPDH. **(E)** RNA was extracted from uninfected WT and *Ifnar1*$^{-/-}$
797 BMM cultures and ISG mRNA were quantified by qRT-PCR. mRNA expression levels relative to β-
798 actin mRNA are expressed as $2^{-\Delta CT}$, where $\Delta C_T = (C_{T,\ \text{Target Gene}} - C_{T,\ \beta\text{-actin}})$. The dashed line
799 designates the lower limit of detection. Data are from pooled from three independent experiments
800 each performed in triplicate and shown as the means ± SEM. *, P < 0.05; **, P < 0.01; ***, P< 0.001;
801 ****, P < 0.0001. **(F)** RNA was extracted from BMM cultures at 9 and 12 hours post infection as well
802 as cultures 12 hours post mock infection and rRNA degradation was assessed with a Bioanalyzer.
803 28S and 18S rRNAs are indicated. **(G)** Astrocytes and microglia, from mixed glial cultures, and
804 macrophages, from bone marrow derived cultures, were stained with cell type specific antibodies, as
805 well as for IFNAR1, analyzed by flow cytometry with an LSR II (Becton Dickinson) and the resulting
806 data were analyzed using FlowJo Software (Treestar). Astrocytes (GFAP^{+}CD11b^{-}F4/80^{-}), microglia
807 (GFAP^{-}CD11b^{+}F4/80^{+}), and macrophages (GFAP^{-}CD11b^{+}F4/80^{+}) were assessed for surface
808 expression of IFNAR1. Data are from one representative experiment of two, each performed with
809 triplicate cultures of each cell type.
810
811 **Figure 6. Activation of RNase L activity in BMM treated with IFNAR1 blocking MAR1-5A3**
812 **mAb.** WT BMM were treated with 2 μg/mL or 5 μg/mL MAR1-5A3 IFNAR1 blocking mAb or no mAb
813 or isotype control Ab (panels E and F only) for 1 hour before infection or mock infection with A59 or
814 ns2^{H126R} (1 PFU/cell). RNA was extracted from cells at 0 time post mock infection and 12 hours post
815 virus infection. Expression levels of **(A)** *Oas1a,* **(B)** *Oas2,* and **(C)** *Oas3* mRNA were quantified by
816 qRT-PCR. Levels of mRNA expression relative to β-actin mRNA are expressed as $2^{-\Delta CT}$, where ΔC_T
817 $= (C_{T,\ \text{Target Gene}} - C_{T,\beta\text{-actin}})$. The dashed line designates the lower limit of detection. These data are
818 pooled from two independent experiments, each performed in triplicate and are shown as the means
819 ± SEM. Values for mock infected, 5 μg/mL mAb treated are significantly different from mock infected,
820 0 mAb or 2 μg/mL mAb treated, *, P <0.05. Supernatants from A59 or ns2^{H126R} infected BMM
821 cultures pretreated with **(D)** no mAb, **(E)** 2 μg/mL IFNAR1 blocking mAb (solid line) or istoype control

822 Ab (dotted line), and **(F)** 5 μg/mL of IFNAR1 blocking mAb (solid line) or istotype control Ab (dotted
823 line) were titered for virus by plaque assay. Data are pooled from three independent experiments
824 (except for isotype control treated cells which was performed one time), each performed in triplicate
825 and are shown as the means ± SEM. *, $P < 0.05$; **, $P < 0.01$. **(G)** RNA was extracted at 9 and 12
826 hours post infection from BMM cultures that had been pretreated with mAb as indicated, and rRNA
827 degradation was assessed with a Bioanalyzer. 28S and 18S rRNAs are indicated. RNA from mock
828 infected cultures appeared similar to that from A59 infected cells (not shown) as in Figures 2E, 3E,
829 4H and 5F.

830
831
832
833
834
835
836
837
838

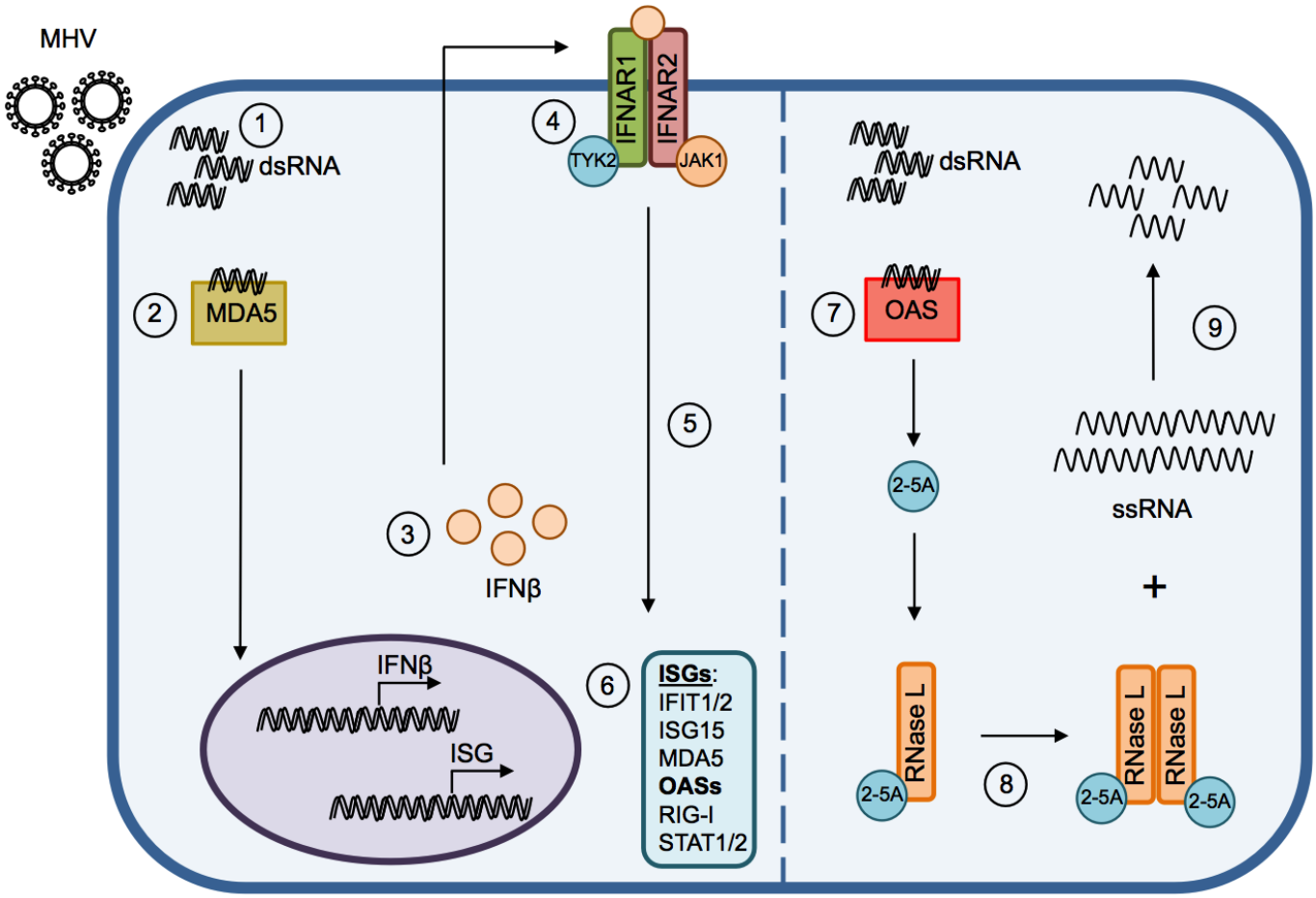

Figure 1

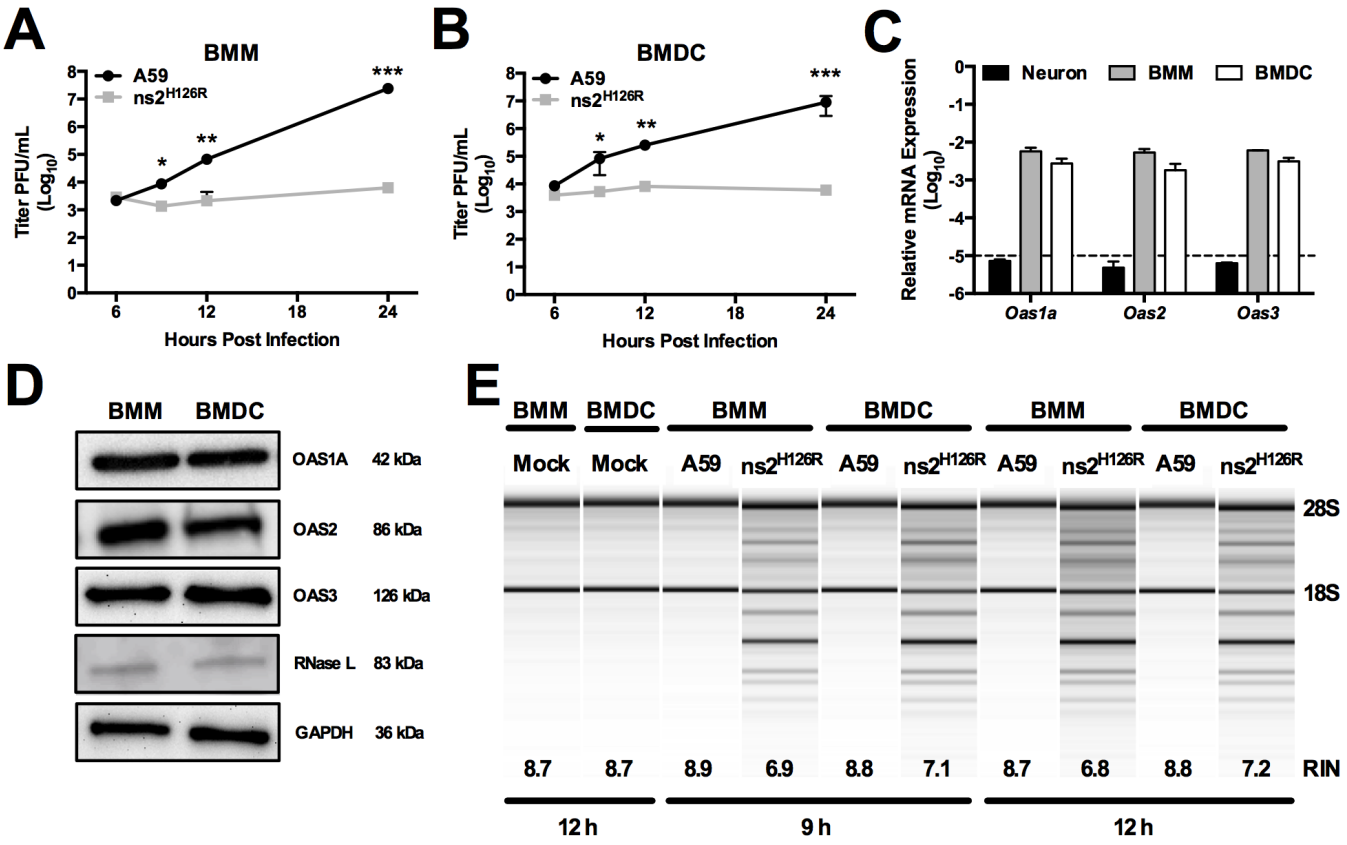

Figure 2

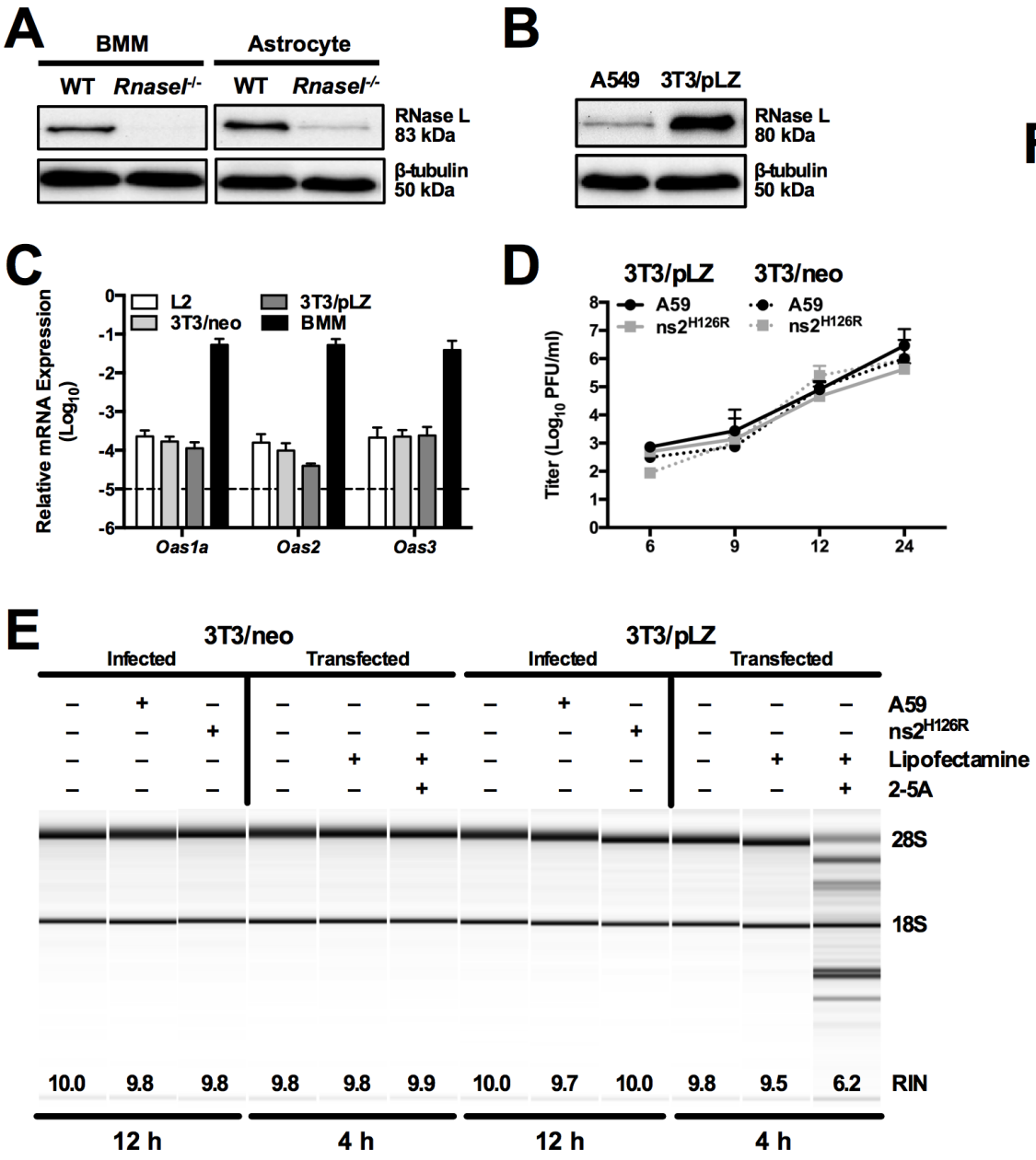

Figure 3

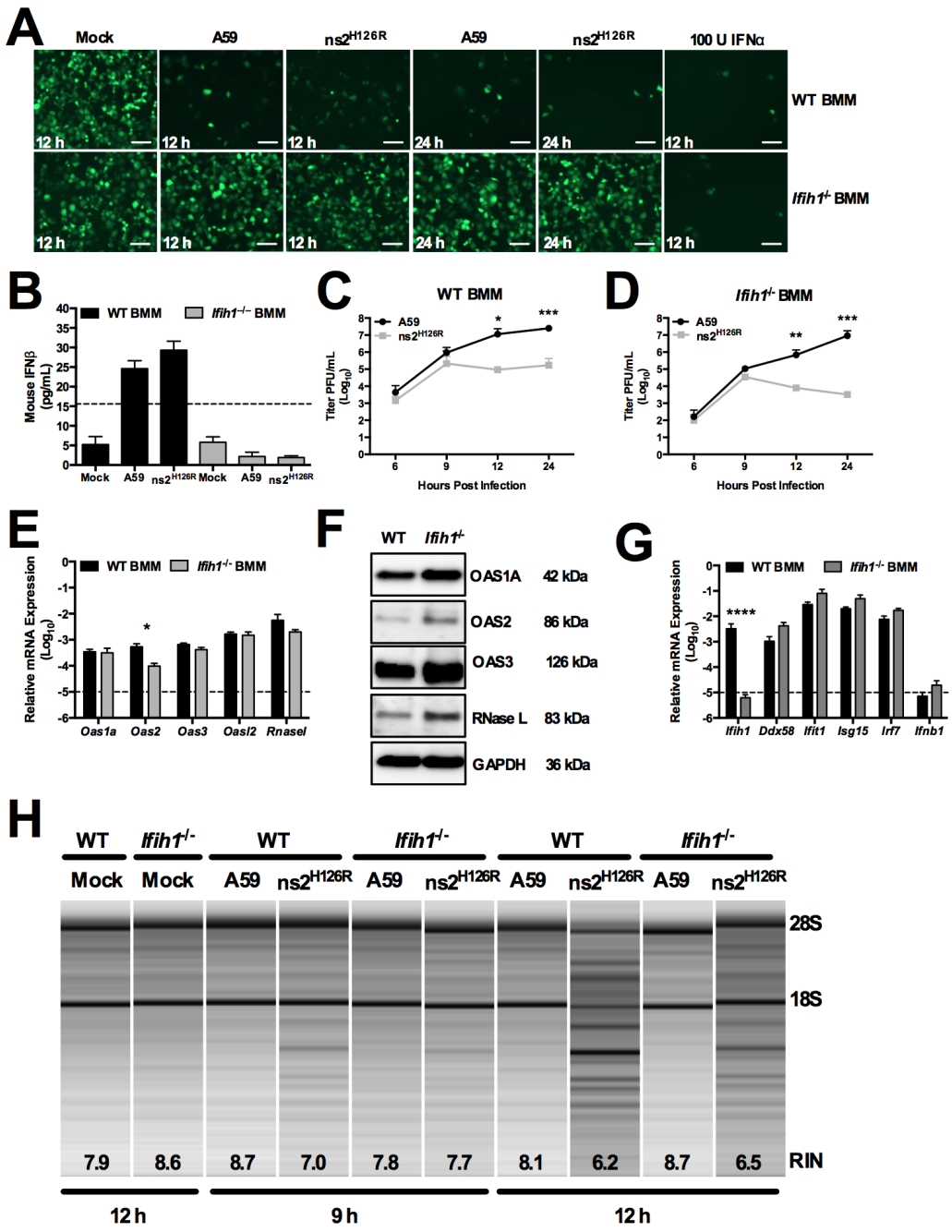

Figure 4

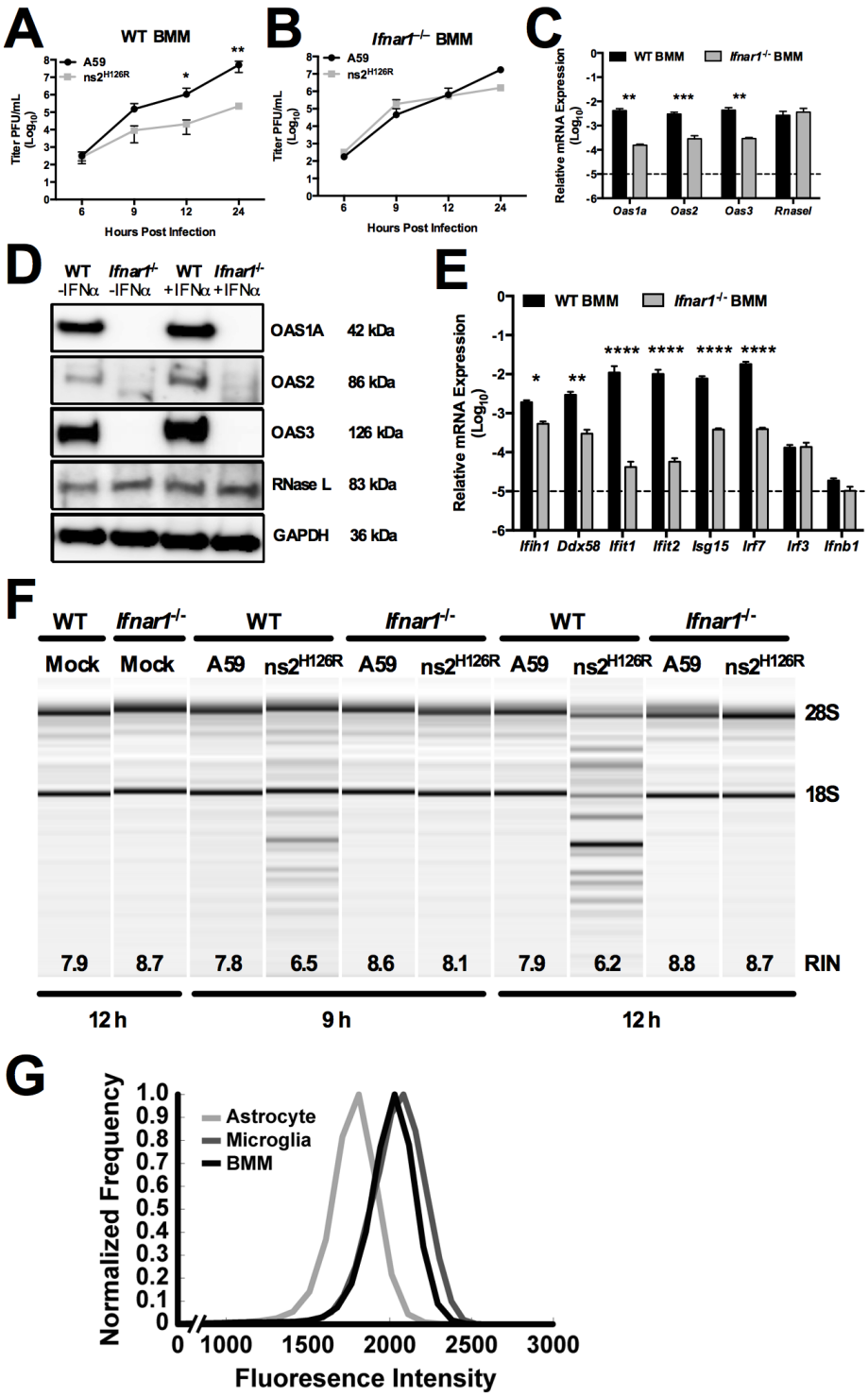

Figure 5

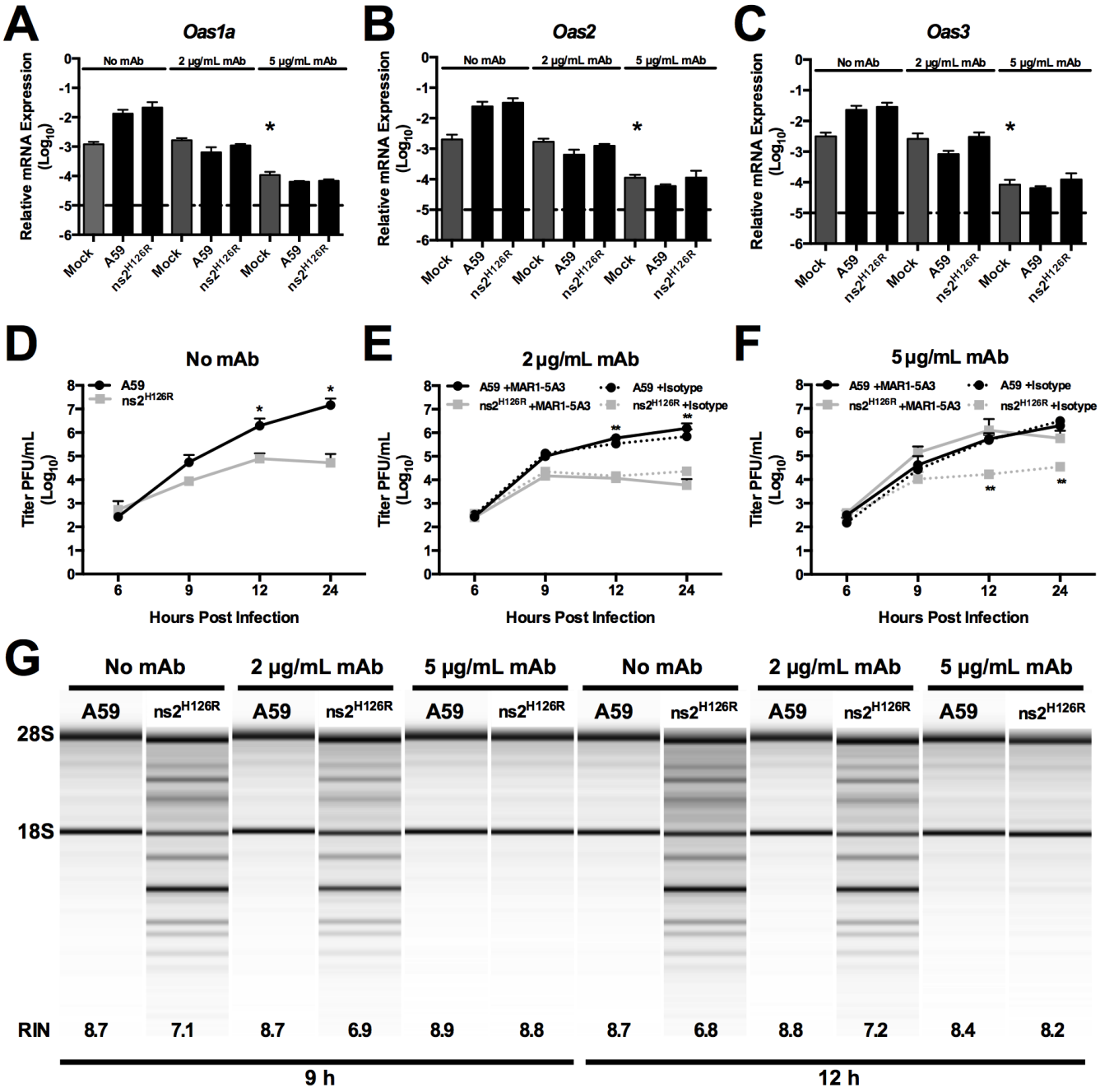

Figure 6